New insights in the structure-activity relationship of 2-phenylamino-substituted benzothiopyrano[4,3-*d*]pyrimidines as kinase inhibitors.

Silvia Salerno [a], Aída Nelly García-Argáez [b], Elisabetta Barresi [a], Sabrina Taliani [a,*], Francesca Simorini [a], Concettina La Motta [a], Giorgio Amendola [c], Stefano Tomassi [c], Sandro Cosconati [c,*], Ettore Novellino [d], Federico Da Settimo [a], Anna Maria Marini [a], Lisa Dalla Via [b].

[a] Dipartimento di Farmacia, Università di Pisa, Via Bonanno 6, 56126 Pisa, Italy.

[b] Dipartimento di Scienze del Farmaco, Università di Padova, Via Marzolo 5, I-35131 Padova, Italy

[c] DiSTABiF, Università della Campania Luigi Vanvitelli, Via Vivaldi 43, 81100 Caserta, Italy.

[d] Dipartimento di Farmacia, Università di Napoli "Federico II", Via D. Montesano 49, 80131 Napoli, Italy.

Abstract

Inhibition of angiogenesis via blocking vascular endothelial growth factor receptor (VEGFR) signaling pathway emerged as an established approach in anticancer therapy. So far, many monoclonal antibodies and ATP-competitive small-molecule inhibitors have been clinically validated and approved. In this study, structure-activity relationships (SAR) within the 2-phenylamino-substituted benzothiopyrano[4,3-*d*]pyrimidine class of kinase inhibitors were further refined by the synthesis and biological evaluation of new compounds **1-21** featuring different substitution patterns on the pendant phenyl moiety, combined with H, OCH$_3$, or Cl at 8-position. Most compounds showed a promising human kinase insert domain receptor (KDR) inhibition profile, with IC$_{50}$ values in the submicromolar/low nanomolar range, and promising antiproliferative activity on human umbilical vein endothelial cells (HUVECs) as well as on a panel of three human tumor cell lines. The angio-kinase selectivity profile was assessed for the most promising compound **16** against a set of six human kinases. Finally, computational studies allowed clarifying at molecular level the interaction pattern established by the compounds with KDR, highlighting key stable cation-π interactions, and thus providing the basis for further designing novel inhibitors.

Keywords: benzothiopyranopyrimidines, KDR kinase, antiproliferative activity, kinase inhibitors.

Abbreviations: A-431, epidermoid carcinoma cell line; DMEDA, *N*,*N*'-dimethylethylendiamine; HeLa, cervix adenocarcinoma cell line; h, human; HUVEC, human umbilical vein endothelial cell; KDR, human kinase insert domain receptor; MSTO-211H, biphasic mesothelioma cell line; SAR, structure-activity relationships; TKR, tyrosine kinase receptor; VEGF, vascular endothelial growth factor; VEGFR, vascular endothelial growth factor receptor.

1. Introduction

Conventional chemotherapeutics have achieved an efficacy plateau against most solid malignancies and exhibit serious side effects. Advances in understanding of tumor biology have led to the development of a novel class of anticancer drugs targeting specific pathways involved in growth, progression and spread of cancer, termed "targeted therapy" [1,2].

Angiogenesis is a pivotal process implicated in tumor growth and metastatic dissemination. In healthy individuals, angiogenesis is strictly limited to short and sporadic time periods such as development, reproduction, and wound healing [3]. However, in the setting of tumor growth, the interplay between co-option of the existing vasculature and tumor angiogenesis becomes an important mechanism for solid tumors to proliferate and metastasize beyond the limits of passive diffusion [4,5]. During pathologic angiogenesis, the balance of pro- and anti-angiogenic factors is shifted to sustained production of proangiogenic factors, leading to the formation of new blood vessels that support the tumor [3].

The vascular endothelial growth factor (VEGF) pathway represents one of the most important positive modulators of angiogenesis, and, within the VEGF family (VEGF-A, VEGF-B, VEGF-C, VEGF-D, VEGF-E), VEGF-A (also termed simply VEGF) is thought to be the most critical in both physiological and pathological angiogenesis [6].

Various members of the VEGF family have similar abilities to interact with a set of highly homologous tyrosine kinase receptors (TKRs): VEGFR-1 (Flt-1) and VEGFR-2 (human KDR or murine Flk-1), largely expressed in endothelial cells, and primarily involved in angiogenesis [7,8]. Therefore, considering the role of the VEGF pathway in angiogenesis, antiangiogenic strategies often involve the use of small molecule tyrosine kinase inhibitors (TKIs) to target one or more of the VEGFRs [9,10]. These TKIs compete with ATP binding in the catalytic domain of the tyrosine kinases, inhibiting kinase activity, thereby preventing activation of downstream signaling cascades.

A number of small-molecule kinase inhibitors targeting primarily VEGFR (e.g. vatalanib, cediranib, axitinib, sorafenib, pazopanib, Chart 1) have been approved or are in development for clinical use [11-13]. In particular, a significant number of VEGFR-2 small molecule inhibitors characterized by a variously substituted pyrimidine or 1,2,4-triazine ring, either isolated or fused to form different heterocyclic structures, have been investigated during the last decade and some of them (e.g., RO4383596 [14], TKI-28 [15], BMS-690514 [16], AZD2932 [17], Chart 2) are in clinical trials for the treatment of different tumors [18,19].
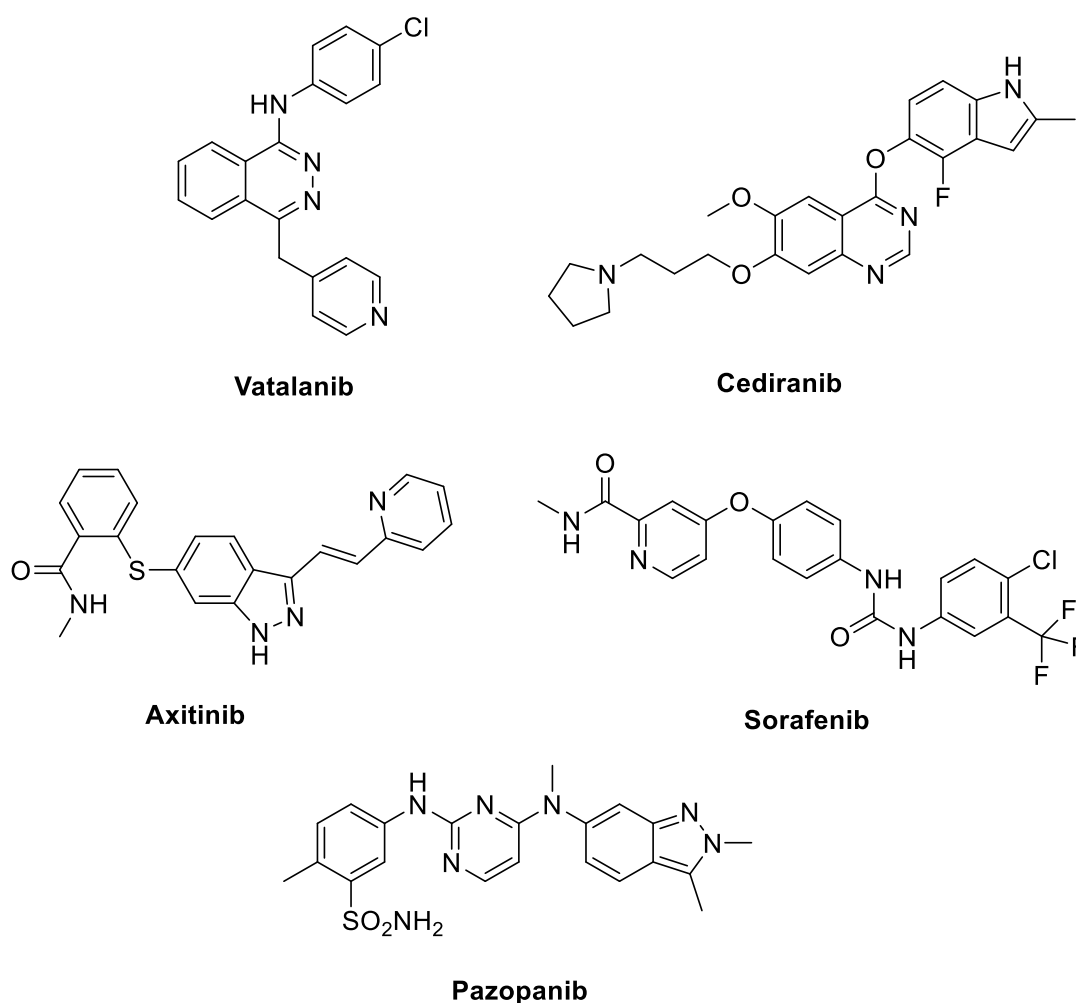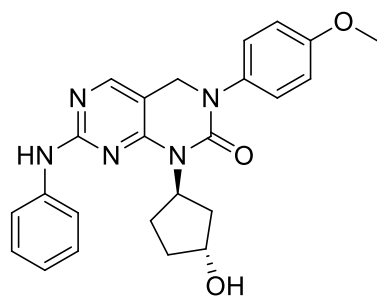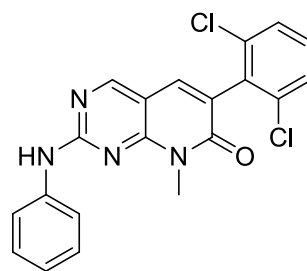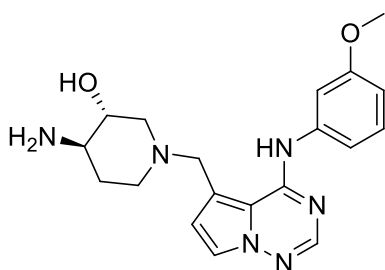

Chart 1. VEGFR Inhibitors clinically approved or in development for the treatment of solid tumors.
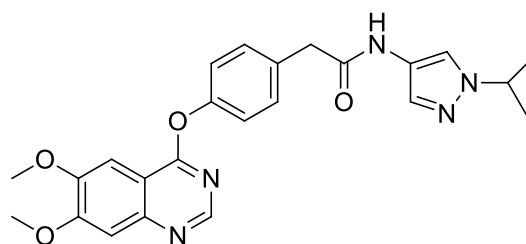
RO4383596

TKI-28

BMS-690514

AZD2932

Chart 2. Pyrimidine- and 1,2,4-triazine-based VEGFR inhibitors in clinical trials.

In this context, we recently reported the synthesis and the biological evaluation of novel antiangiogenic agents featuring the benzothiopyrano[4,3-*d*]pyrimidine scaffold decorated with a pendant benzylamino or phenylamino moiety (**A** and **B**, respectively, Chart 3) [20], whose design was based on the structures of some anilino-substituted pyrimidines reported as inhibitors of protein kinases [21]. In particular, compounds bearing a phenyl-amino side group at the 2-position of the tricyclic system (**B**, Chart 3) emerged as the most interesting ones, many of these displaying a promising inhibitory profile on both human kinase insert domain receptor (KDR) and human umbilical vein endothelial cells (HUVECs), with IC_{50} and GI_{50} values, respectively, in the low micromolar range [20]. All in all, these studies suggested that the new 2-anilino substituted heteropolycyclic moiety could be worth of further structural investigation.

According to our initial molecular docking studies [20], the benzothiopyranopyrimidine scaffold is inserted in the hydrophobic ATP cleft of the enzyme active site. Here, the ligand would be able to

5

establish a double H bond with its nitrogen at 3-position and the adjacent aniline NH at 2-position with the backbone NH and CO of Cys919, respectively. Moreover, according to our previous work, while the ligand aniline NH would be critical for ligand binding, bulky substituents at 8-position have a detrimental effect.

A close inspection of our already published theoretical interaction model [20] also reveals the presence of Lys838 and Phe1047 residues that could provide further interaction points. In principle, contacts with these latter residues could be further enhanced by designing new benzothiopyranopyrimidine analogues with potentially higher inhibitory activities.

Based on all these considerations, with the aim of further investigating the structure-activity relationships (SAR) of these 2-anilino-substituted benzothiopyranopyrimidines for the development of novel kinase inhibitors acting as antiangiogenic agents, we designed, synthesized and biologically evaluated new compounds, featuring different substitution patterns on the pendant phenyl moiety, combined with an H, OCH_3, or Cl at 8-position (1-21, Chart 3). The groups on the pendant phenyl ring were selected taking into account literature data about small molecules kinase inhibitors, featuring meta- or poly-substituted aniline or phenyl moieties [22-24].
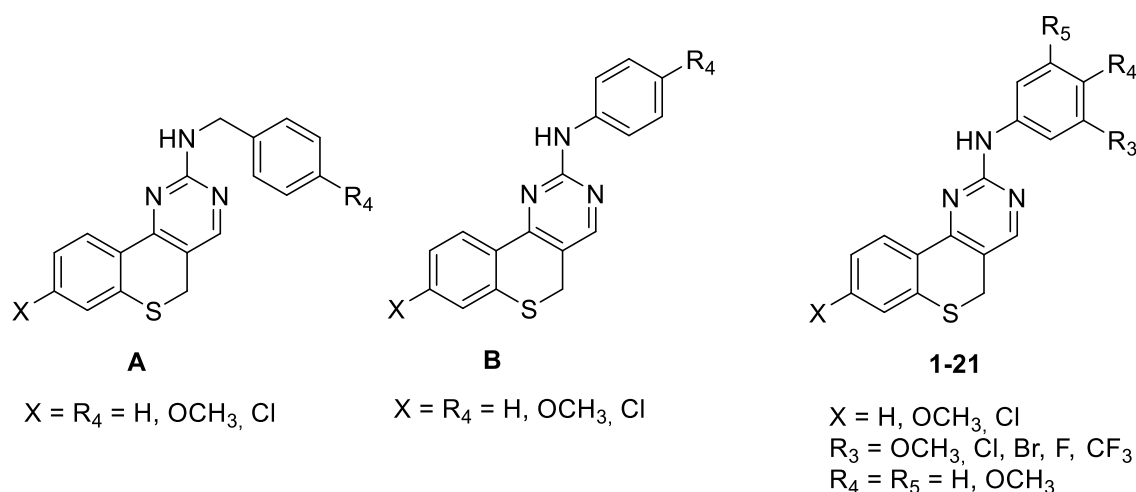

Chart 3. Structures of previously reported (**A**, **B**) [20], and newly synthesized benzothiopyranopyrimidines (**1-21**).

The ability of the new synthesized benzothiopyranopyrimidines **1-21** to inhibit the kinase activity of the KDR was determined by a fluorimetric assay designed to detect and characterize kinase inhibitors. In addition, the antiproliferative activity of the compounds on HUVECs and on a panel of human tumor cell lines (HeLa, A-431, and MSTO-211H) was evaluated. For the most promising compound **16**, the angio-kinase selectivity profile was assessed against a set of six human kinases. Finally, molecular docking calculations allowed clarifying at molecular level the proposed interaction pattern established by the compounds with KDR.

2. Results and Discussion

2.1. Chemistry

The intermediates in the synthesis of target compounds **1-21** were the 2-aminopyrimidino derivatives **24a-c**, which were prepared by a previously reported two-steps procedure (Scheme 1) [20]. Briefly, reaction of 7-substituted-2,3-dihydrobenzo[3',2':5,6]thiopyrano-4(4H)-ones **22a-c** with an excess of dimethylformamide dimethylacetal (DMF DMA) in refluxing toluene furnished the 3-dimethylaminomethylene derivatives **23a-c** [20,25]. Intermediates **23a-c** were then treated with guanidine hydrochloride, in the presence of sodium ethoxide in refluxing ethanol, to obtain the 2-aminopyrimidino derivatives **24a-c**, with good yields [20]. Finally, compounds **24a-c** were allowed to react with the commercially available appropriately substituted phenyliodide in anhydrous dioxane, under nitrogen atmosphere and in the presence of K$_2$CO$_3$, N,N'-dimethylethylendiamine and CuI, affording the crude **1-21,** which were purified by flash chromatography, using petroleum ether 60-80 °C/ethyl acetate 5:5 as the eluting system for all the compounds.

All the target derivatives showed high purity and the proposed structures were confirmed on the basis of ^{1}H-NMR, ^{13}C-NMR, and HMRS data.

Scheme 1
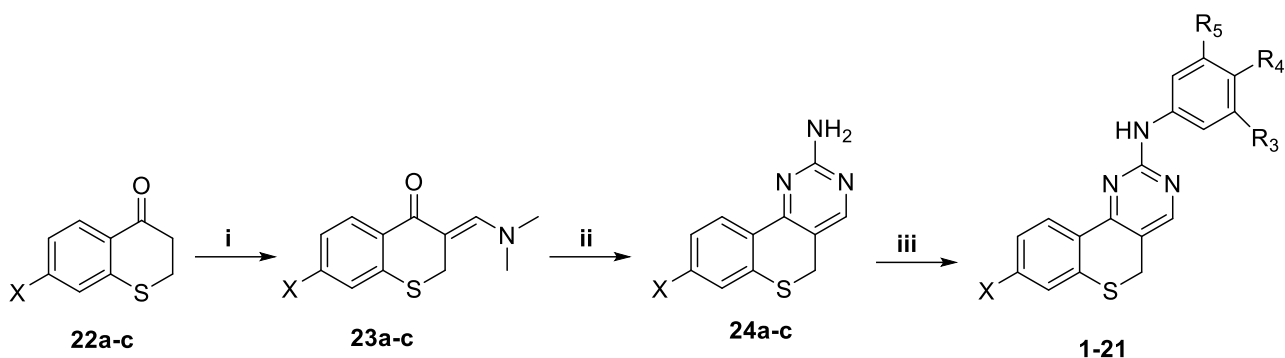
22a-24a: X = H
22b-24b: X = OCH₃
22c-24c: X = Cl

1: X = H, R₃ = OCH₃, R₄ = R₅ = H	**11**: X = Cl, R₃ = OCH₃, R₄ = R₅ = H
2: X = H, R₃ = Cl, R₄ = R₅ = H	**12**: X = Cl, R₃ = Cl, R₄ = R₅ = H
3: X = H, R₃ = Br, R₄ = R₅ = H	**13**: X = Cl, R₃ = Br, R₄ = R₅ = H
4: X = H, R₃ = F, R₄ = R₅ = H	**14**: X = Cl, R₃ = F, R₄ = R₅ = H
5: X = H, R₃ = CF₃, R₄ = R₅ = H	**15**: X = Cl, R₃ = CF₃, R₄ = R₅ = H
6: X = OCH₃, R₃ = OCH₃, R₄ = R₅ = H	**16**: X = H, R₃ = R₄ = OCH₃, R₅ = H
7: X = OCH₃, R₃ = Cl, R₄ = R₅ = H	**17**: X = H, R₃ = R₄ = R₅ =OCH₃
8: X = OCH₃, R₃ = Br, R₄ = R₅ = H	**18**: X = R₃ = R₄ = OCH₃, R₅ = H
9: X = OCH₃, R₃ = F, R₄ = R₅ = H	**19**: X = R₃ = R₄ = R₅ = OCH₃
10: X = OCH₃, R₃ = CF₃, R₄ = R₅ = H	**20**: X = Cl, R₃ = R₄ = OCH₃, R₅ = H
	21: X = Cl, R₃ = R₄ = R₅ = OCH₃

Reagents and conditions: (i) dimethylformamide dimethylacetal (DMF DMA), refluxing toluene, **(ii)** guanidine hydrochloride, EtONa, refluxing ethanol; **(iii)** 3-substituted, 3,4-dimethoxy or 3,4,5-trimethoxy phenyliodide, K₂CO₃, *N,N'*-dimethylethylendiamine (DMEDA), CuI, dioxane.

2.2. Biological evaluation

2.2.1. Effect on KDR kinase activity

The ability of **1-21** to inhibit the KDR kinase activity was determined on a recombinant human kinase insert domain receptor, by using a fluorimetric assay.

Table 1 lists the activity of benzothiopiranopyrimidines **1-21**, together with that of representative compounds from series **B** (**2a-i**). for comparison purposes. Semaxanib was taken as reference compound because of its selectivity in inhibiting VEGFR-1 and -2 and VEGF-dependent endothelial proliferation as compared with other well known tyrosine kinase inhibitors [26]. The results are expressed as inhibition percentage at 7 µM concentration or as IC₅₀ values for the most active compounds.
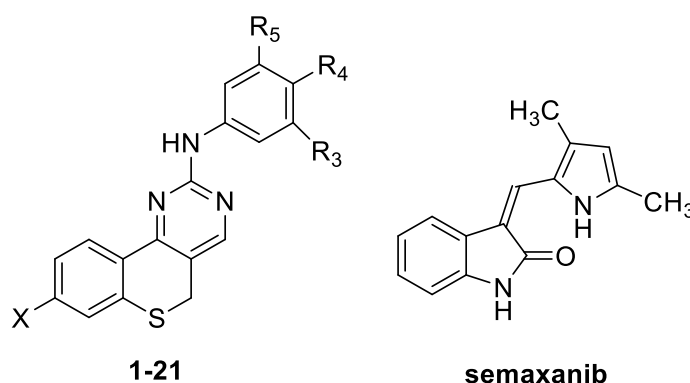
An interdependent effect on KDR inhibition of the meta-substituent on the pendant anilino phenyl ring and the substitution pattern at the 8-position of the tricyclic scaffold can be observed for compounds **1-15**. Specifically, within the 8-unsubstituted subset (compounds **1-5**), the shift of the methoxy group from para (**2b**) to meta position (**1**) produces a gain in inhibitory efficacy against the target protein. In general, the replacement of the methoxy with Cl, Br or CF_3 groups (**2**, **3** and **5**, respectively) decreases drastically the activity. The sole exception to this trend is represented by the fluorine-substituted ligand **4** that shows a 52% of inhibition, which is slightly higher with respect to that of by semaxanib, but still lower than the activitiy displayed by the methoxy-substituted compound **1**. Interestingly, most derivatives from the 8-methoxy subset (**6-10**) show good to high inhibitory efficacy, with percentage values of inhibition comparable or higher than that of the reference. In this case, the most active compound **8** features the 3′-bromo-8-methoxy substitution pattern and notably, it is able to induce an almost complete inhibition at the considered concentration. Conversely, the presence of a chlorine (**7**) or a fluorine (**9**) yields 3′-substituted compounds showing inhibitory efficacy significantly lower with respect to **8** and comparable to that of semaxanib. The insertion of a chlorine at 8 position gives the subset **11**-**15** that shows an inhibitory trend similar to those of the unsubstituted **1**-**5**. In particular, the presence of a methoxy group or a fluorine atom at the meta (3') position enables an effect on KDR. In this case, for both compounds the percentage of inhibition is comparable to that of semaxanib. Otherwise, Cl, Br or CF_3 groups render the 8-chloro-substituted benzothiopiranopyrimidines unable to induce any effect on the kinase activity of the enzyme.

Noteworthy, very interesting results regarding the role of the different substituents on KDR inhibition were obtained by the insertion of two methoxy groups in R3 and R4 on the phenyl ring of the side chain and by the presence or the absence of the same group in 8 (compounds **16-21**). Actually, the 8-unsubstituted and 8-Cl derivatives (**16, 17**, **20, 21**), are the most active of the whole series probably due to electronic effects that favor charge transfer interactions with the target protein. In contrast, for the 8-OCH_3 substituted derivatives **18** and **19**, an inhibitory effect is observed, probably due to an

excessive dimension of the whole molecule that determines its relocation in the enzyme active site and, consequently, the loss of crucial interactions with the protein, in agreement with previous findings [20].

The activity of the best performing derivatives was also confirmed by the determination of the IC_{50} values (Table 1). The results highlighted for all the most active compounds **1**, **8**, **16**, **17**, **20** and **21** a very interesting capacity to inhibit the enzyme, with IC_{50} values ranging from 0.11 to 1.6 µM significantly lower with respect to the values obtained for both the most active of the previously reported benzothiopyranopyrimidines (**2b**) and the reference compound (semaxanib, $IC_{50} = 12.9$ µM). Of note, **16** and **17** (3′,4′-dimethoxy- and 3′,4′,5′-trimethoxy-substituted, respectively) displayed a 24- and 10-fold increase in KDR inhibitory activity (expressed as IC_{50} value) with respect to their parent compound **2b**, further supporting the beneficial effect produced by the methoxy groups.

Table 1. KDR enzyme inhibitory activity and HUVEC growth inhibition of derivatives **1**-**21** and semaxanib as reference compound.

cpd	X	R_3	R_4	R_5	KDR (%)[a]	KDR IC_{50} (µM)[b]	HUVEC GI_{50} (µM)
2a[d]	H	H	H	H	54	8.20	2.40
2b[d]	H	H	OCH_3	H	67	2.70	0.45
2c[d]	H	H	Cl	H	<20	>50	7.30
2d[d]	OCH_3	H	H	H	35	>50	4.30
2e[d]	OCH_3	H	OCH_3	H	39	17.50	0.74
2f[d]	OCH_3	H	Cl	H	<20	>50	>20
2g[d]	Cl	H	H	H	<20	>50	>20

2h[d]	Cl	H	OCH$_3$	H	<20	>50	16.40
2i[d]	Cl	H	Cl	H	61	5.60	0.35
1	H	OCH$_3$	H	H	75	0.97	0.80
2	H	Cl	H	H	<20	n.d.	7.13
3	H	Br	H	H	<20	n.d.	7.00
4	H	F	H	H	52	n.d.	4.51
5	H	CF$_3$	H	H	<20	n.d.	5.02
6	OCH$_3$	OCH$_3$	H	H	62	n.d.	2.49
7	OCH$_3$	Cl	H	H	40	n.d.	11.19
8	OCH$_3$	Br	H	H	93	0.62	1.89
9	OCH$_3$	F	H	H	35	n.d.	11.48
10	OCH$_3$	CF$_3$	H	H	21	n.d.	4.55
11	Cl	OCH$_3$	H	H	44	n.d.	14.17
12	Cl	Cl	H	H	<20	n.d.	16.51
13	Cl	Br	H	H	<20	n.d.	7.11
14	Cl	F	H	H	42	n.d.	18.23
15	Cl	CF$_3$	H	H	<20	n.d.	10.46
16	H	OCH$_3$	OCH$_3$	H	97	0.11	1.50
17	H	OCH$_3$	OCH$_3$	OCH$_3$	81	0.27	1.99
18	OCH$_3$	OCH$_3$	OCH$_3$	H	<20	n.d.	10.82
19	OCH$_3$	OCH$_3$	OCH$_3$	OCH$_3$	46	n.d.	3.71
20	Cl	OCH$_3$	OCH$_3$	H	87	0.73	2.53
21	Cl	OCH$_3$	OCH$_3$	OCH$_3$	73	1.60	2.54
semaxanib[d]	-	-	-	-	40	12.90	13.60

[a] Percentage of kinase inhibition obtained at 7 µM of the test compound. [b] IC$_{50}$ values represent the concentration that induces the 50% reduction in enzyme activity. [c] GI$_{50}$ values represent the concentration (µM) of compound able to produce 50% cell death with respect to the control culture. [d] Data from ref. [20].

2.2.2. Growth inhibition on HUVEC cells

The new benzothiopyranopyrimidine derivatives **1-21** were evaluated for their effect on cell growth of HUVEC cells.

The results, expressed as GI$_{50}$ values, i.e. concentration (µM) able to induce 50% cell death with respect to a control culture, are shown in Table 1. Semaxanib was used as reference compound. After a 72h exposure, the majority of the newly synthesized benzothiopyranopyrimidines exert a detectable antiproliferative effect on HUVEC cells, with GI$_{50}$ values ranging in the low micromolar range (from

0.80 to 18.2 µM). Interestingly, a comparison between the antiproliferative effect exerted by **1-21** and their ability to inhibit the kinase activity of KDR highlighted a noteworthy positive correlation. Indeed, among the newly investigated benzothiopyranopyrimidine derivatives **1-21**, the compounds that resulted more potent in KDR inhibition (**1**, **8**, **16**, **17**, **20**, **21**) also showed low GI$_{50}$ values. In particular, for the most potent benzothiopyranopyrimidine **16** both the IC$_{50}$ and GI$_{50}$ values are several folds lower than the corresponding values recorded for semaxanib (see Table 1).

2.2.3. Antiproliferative activity on human tumor cell lines.

The antiproliferative activity of benzothiopyranopyrimidine derivatives **1-21** against a panel of human tumor cell lines, HeLa (cervix adenocarcinoma), A-431 (epidermoid carcinoma) and MSTO-211H (biphasic mesothelioma), was evaluated to define their cell proliferation profile.

The results, expressed as GI$_{50}$ values, are shown in Table 2 and semaxanib was taken into consideration as reference. The obtained results highlighted for the majority of the newly synthesized derivatives evident cytotoxic effects, as demonstrated by the GI$_{50}$ values in the micromolar range. Cell growth evaluation revealed again a positive effect attributable to a poly-methoxy substitution on the pendant phenyl ring: molecules from the subseries **16-21** are highly cytotoxic derivatives, with the exception of **18**. Interestingly, **19** proved to be one the most antiproliferative compound, despite its low percentage of KDR inhibition, suggesting that its activity is probably mediated by interactions with other molecular targets.

Overall, the results shown in Table 2 appear roughly in accordance with those of Table 1, suggesting the activity of benzothiopyranopyrimidine derivatives is mainly mediated by KDR inhibition, although interference with additional biological targets and/or kinases cannot be excluded.

Table 2. Cell growth inhibition of derivatives **1-21** and semaxanib as reference compound.

cpd	X	R$_3$	R$_4$	R$_5$	GI$_{50}$ (µM)[a]		
					HeLa	A-431	MSTO-211H

1	H	OCH$_3$	H	H	6.03±1.81	9.43±0.21	0.80±0.14
2	H	Cl	H	H	>20	10.4±1.8	6.10±1.44
3	H	Br	H	H	>20	10.6±1.6	7.67±1.26
4	H	F	H	H	14.0±2.1	9.76±0.68	2.06±1.04
5	H	CF$_3$	H	H	>20	13.5±2.1	11.8±2.5
6	OCH$_3$	OCH$_3$	H	H	2.80±0.44	2.10±0.36	2.57±0.87
7	OCH$_3$	Cl	H	H	11.9±1.8	8.25±2.72	5.60±1.27
8	OCH$_3$	Br	H	H	2.93±0.51	4.77±0.42	2.20±0.30
9	OCH$_3$	F	H	H	10.3±1.6	15.5±1.4	13.0±1.3
10	OCH$_3$	CF$_3$	H	H	6.02±0.46	6.24±0.42	9.04±0.52
11	Cl	OCH$_3$	H	H	>20	16.8±1.6	6.83±1.36
12	Cl	Cl	H	H	>20	>20	7.78±1.26
13	Cl	Br	H	H	>20	17.0±1.4	8.50±1.14
14	Cl	F	H	H	20	18.2±1.5	>20
15	Cl	CF$_3$	H	H	>20	10.0±0.6	3.18±0.28
16	H	OCH$_3$	OCH$_3$	H	1.50±0.29	2.32±0.41	1.63±0.35
17	H	OCH$_3$	OCH$_3$	OCH$_3$	1.26±0.17	1.92±0.31	1.08±0.19
18	OCH$_3$	OCH$_3$	OCH$_3$	H	18.8±1.2	6.06±1.16	>20
19	OCH$_3$	OCH$_3$	OCH$_3$	OCH$_3$	0.63±0.15	1.75±0.44	0.92±0.13
20	Cl	OCH$_3$	OCH$_3$	H	3.42±0.44	2.23±0.71	4.40±1.15
21	Cl	OCH$_3$	OCH$_3$	OCH$_3$	3.46±0.45	4.27±0.50	3.40±1.10
semaxanib	-	-	-	-	38±1	37±3	27±2

[a] GI$_{50}$ values represent the concentration (μM) of compound able to produce 50% cell death with respect to the control culture.

2.2.4 Effect on human kinases

To investigate the possibility that other kinases, apart from KDR, could be affected by the new benzothiopyranopyrimidine derivatives, the selectivity profile of compound **16**, the most active compound in inhibiting KDR, was determined. For this purpose, the effect of **16** was further assessed against a set of six human (h) kinases, i.e. AurA/Aur2 kinase, CDC2/CDK1, EGFR kinase, PDGFRβ kinase, RAF-1 kinase and Src kinase, which are reported to be mainly involved in cell proliferation. The obtained results suggest **16** as a multi-target inhibitor, because, besides KDR, it is able, analogously to what previously reported for the parent compound **2b** [20], to inhibit to a significant extent also Aurora (AurA/Aur2) kinase, a nuclear serine/threonine protein kinase involved in many

functions related to mitosis (Figure 1, Tables S1a, and S1b) [27]. Moreover, a relevant inhibitory effect occurs toward the non-receptor tyrosine kinase Src. The multiplicity of kinase targets of **16** could explain the ability of this compound to inhibit along with HUVEC cells also a number of other human tumor cell lines.
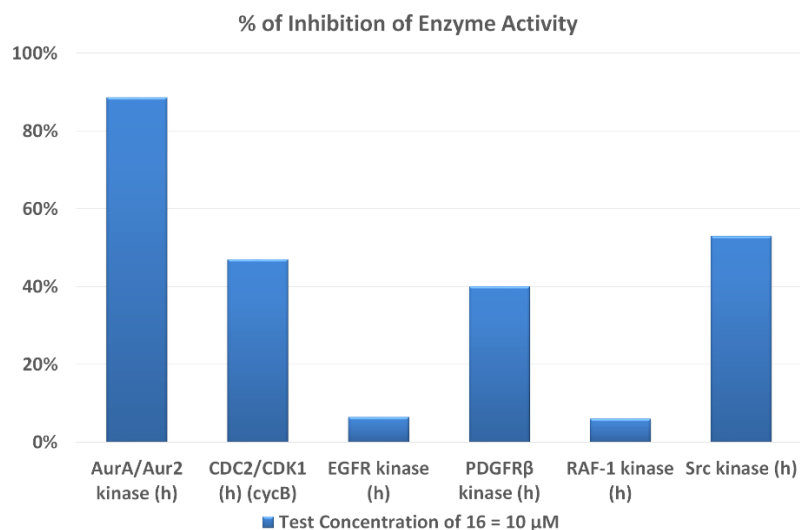

Figure 1. Percentage of inhibition of kinase activity in the presence of compound **16**.

2.3. Molecular Modeling.

To elucidate the possible reasons behind the displayed activity of the newly designed compounds, molecular docking studies were performed. The calculations were executed with the AutoDock Vina software [28], employing an ensemble approach, which has been proven to be a successful way to accurately predict the correct ligand binding poses [29-31] in the case of pronounced protein plasticity upon ligand binding. Namely, the most active compound, **16**, was docked to all the available crystal structure of VEGFR2 with a resolution below 2 Å (see molecular modeling methods for PDB codes). The docked poses were visually inspected for correct geometries. According to these simulations **16** was predicted to form the most stable complex with the published VEGFR2 crystal having PDB code 3EWH [32] as indicated by the calculated binding free energy (ΔG_{VINA}= -8.7 kcal/mol). In this

structure, the activation loop of the enzyme adopts the inactive DFG-out conformation.

Interestingly, the **16** docked pose is consistent with our previous findings on the parent compound **2b** [20]. The benzothiopyranopyrimidine scaffold is well positioned in the ATP binding site to establish a double H-bond with the backbone NH and CO of Cys919 on the hinge region through its nitrogen at position 3 and the adjacent exocyclic NH at position 2 (Figure 2a). The tricyclic system engages favorable contacts with the hydrophobic cleft which comprises Leu840, Val848, Ala866, Val899, and Leu1035. Moreover, charge transfer interactions are established with Phe918 and Phe1047. Of note, the ligand pendant anilino phenyl ring is oriented outwards of the binding pocket and is stabilized by a cation-π interaction with the Lys838 side-chain.
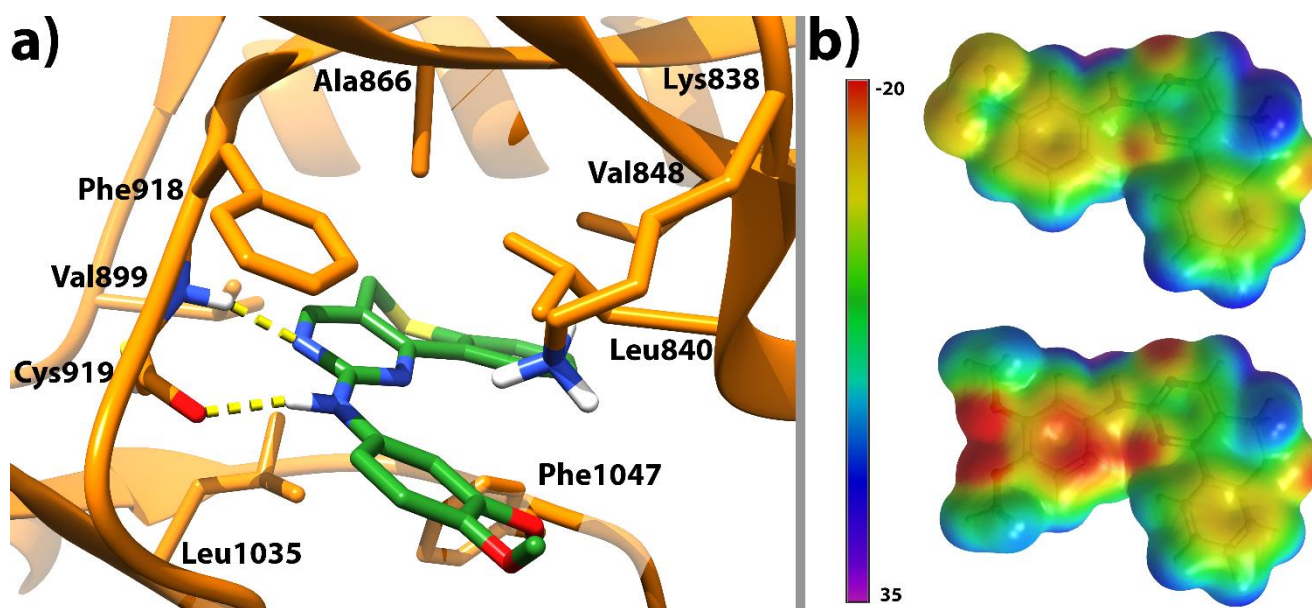

Figure 2. (a) Binding mode of compound **16**, within the VEGFR-2 active site (PDB code 3EWH). The ligand is represented as green sticks while the protein as orange sticks and ribbons. H-bonds are depicted as dashed yellow lines. The picture was rendered with the UCSF Chimera software [33]. **(b)** Electrostatic potentials of compounds **5** and **16** mapped onto their electron density, with a scale of −20.0 (red) to 35.0 kcal/mol (blue).

The occurrence of such an interaction would explain the influence of the substitution pattern of the

pendant aniline ring on the VEGFR inhibition activity. Indeed, electron-donating substituents generally increase the negative electrostatic potential of the aromatic ring, thereby enhancing the charge transfer interaction [34]. This should account for the relatively high inhibition potential displayed by compounds **1**, **16**, **17**, **20**, **21** featuring one, two or three methoxy groups. On the other hand, the insertion on the phenyl ring of electron-withdrawing substituents should weaken the cation-π interaction and is therefore generally detrimental for the inhibitory potency. This should explain why congeners featuring Cl, F, Br, and CF_3 (**2**, **3**, **4**, **5**) show low inhibition towards the enzyme. The influence of the substitution pattern on the electron-availability of the pendant anilino moiety is clearly evidenced in Figure 2b where the electrostatic potentials, calculated through *ab initio* calculations, of an inactive congener (**5**) and of the most active of the series (**16**) are reported.

In general, substitutions at position 8 are not well tolerated, probably due to the limited extension of the cleft, which does not enable the allocation of bulky substituents, with the sole exception to this trend being the submicromolar inhibitory activity displayed by compound **8**.

3. Conclusions

To further investigate the SAR of the 2-anilino-substituted benzothiopyranopyrimidine class of kinase inhibitors for the development of novel antiangiogenic agents, a library of novel derivatives featuring different substitution patterns on the pendant phenyl moiety, combined with H, OCH_3, or Cl at 8-position, was synthesized and biologically evaluated.

Many compounds showed a promising KDR inhibition profile, with IC_{50} values (determined only for those derivatives displaying the highest inhibition percentages) in the submicromolar/low micromolar range (from 0.11 to 1.6 µM), significantly lower with respect to those obtained for both the most active of the previously reported benzothiopyranpyrimidines (**2b**) and the reference compound (semaxanib, IC_{50} = 12.9 µM). The most interesting results in terms of KDR inhibition were obtained by the insertion of two or three methoxy groups on the pendant phenyl ring combined with 8-H and 8-Cl substitution (**16, 17**, **20**, **21**), with **16** being the best performing compound of the whole series.

SAR data were rationalized by the creation of a theoretical ligand/enzyme complex. Visual inspection of such a complex suggest that electron-donating substituents (such as methoxy) on the aniline ring would enhance the charge transfer interaction with the target protein thereby producing a beneficial effect on KDR inhibition activity.

All the new benzothiopyranopyrimidine derivatives were evaluated for their effect on cell growth of human umbilical vein endothelial primary cells (HUVECs), and a panel of human tumor cell lines, HeLa (cervix adenocarcinoma), A-431 (epidermoid carcinoma) and MSTO-211H (biphasic mesothelioma). The majority of these compounds exert evident cytotoxic effects (GI_{50} values in the low micromolar range), revealing again a positive effect ascribable to a poly-methoxy substitution on the pendant phenyl ring.

Finally, selectivity profile of compound **16** has been assessed against a set of six human kinases (AurA/Aur2 kinase, CDC2/CDK1, EGFR kinase, PDGFRβ kinase, RAF-1 kinase and Src kinase) to investigate the possibility that other kinases could be involved in its biological activity. Actually, the obtained results suggested **16** as a multi-target inhibitor, analogously to what previously reported for its parent compound **2b** [20].

Taken together, these data corroborate the 2-anilino-substituted benzothiopyrano moiety as an interesting structure inside the field of kinase-targeted antitumor agents, providing the platform for further structural optimization aimed to obtain increasingly potent TK inhibitors.

4. Experimental protocols

4.1.Chemistry

The uncorrected melting points were determined using a Reichert Köfler hot-stage apparatus. ^{1}H NMR spectra were recorded on a Bruker AVANCE 400 (^{1}H, 400 MHz, ^{13}C, 100 MHz) in DMSO-d_6 (internal standard tetramethylsilane). The coupling constants (*J*) are given in Hertz. Accurate molecular weights of compounds were confirmed by ESI mass spectrometry using a Q Exactive Orbitrap LC−MS/MS (Thermo Fisher Scientific, Waltham, MA, USA). Analytical TLC have been

carried out on Merck 0.2 mm precoated silica gel aluminium sheets (60 F-254). Silica gel 60 (230–400 mesh) was used for column chromatography. Purity of the target inhibitors **1-21** was determined using a Shimadzu LC-20AD SP liquid chromatograph equipped with a DDA Detector set at 204 nm and 280 nm (column C18 (250 mm x 4.6 mm, 5 μm, Shim-pack)); the mobile phase, delivered at isocratic flow, consisted of methanol (80%) and water (20%) and a flow rate of 1.0 mL/min; all the compounds showed percent purity values of >95%. The combustion analyses of compounds **1-21** are indicated by symbols, and the analytical results are within ± 0.4% of the theoretical values. Reagents, starting materials, and solvents were purchased from commercial suppliers and used as received. 2,3-Dihydrobenzo[3',2':5,6]thiopyrano-4(4*H*)-one **22a** and 7-methoxy-2,3-dihydrobenzo[3',2':5,6]thiopyrano-4(4*H*)-one **22b** were commercially available. The following compounds were obtained according to methods previously described: 7-chloro-2,3-dihydrobenzo[3',2':5,6]thiopyrano-4(4*H*)-one **22c** [25]; 3-Dimethylaminomethylen-2,3-dihydrobenzo[3',2':5,6]thiopyran-4(4*H*)-one **23a**, 7-Methoxy-3-dimethylaminomethylen-2,3-dihydrobenzo[3',2':5,6]thiopyran-4(4*H*)-one **23b** and 7-Chloro-3-dimethylaminomethylen-2,3-dihydrobenzo[3',2':5,6]thiopyran-4(4*H*)-one **23c** [25]; 2-Amino-5H-benzo[3',2':5,6]thiopyrano[4,3-*d*]pyrimidine **24a**, 2-Amino-8-methoxy-5*H*-benzo[3',2':5,6]thiopyrano[4,3-*d*]pyrimidines **24b** and [2-Amino-8-chloro-5*H*-benzo[3',2':5,6]thiopyrano[4,3-*d*]pyrimidine **24c** [20,25].

4.1.1. General synthetic procedures for 2-Anilino-5H-benzo[3',2':5,6]thiopyrano[4,3-d]pyrimidines 1-21

The appropriate 2-amino-5*H*-benzo[3',2':5,6]thiopyrano[4,3-d]pyrimidine **22a-c** (0.417 mmol) was added, at room temperature, under nitrogen atmosphere, to 0.079 g of CuI (0.417 mmol) and 0.115 g of anhydrous K_2CO_3 (0.833 mmol). Then, the appropriate substituted aryl iodide (0.694 mmol), 0.04 mL of DMEDA (0.417 mmol) and 2.5 mL of dioxane were added. The reaction mixture was heated at 100 °C and allowed to stir for 24 h. After cooling, the reaction mixture was added with 2.5 mL of concentrated NH_3 and with a saturated solution of NaCl (10-15 mL). The mixture was extracted with

ethyl acetate. The organic phase was dried (MgSO$_4$) and evaporated under reduced pressure giving a residue which was purified by flash chromatography using petroleum ether 60-80°C/ethyl acetate 5:5 as the eluting system, to give compounds **1-21**.

*4.1.1.1. 2-(3-Methoxyanilino)-5H-benzothiopyrane[4,3-d]pyrimidine (**1**).* Yield: 30%; m. p. 136-137 °C; ^{1}H NMR (400 MHz, DMSO-d$_6$): δ 3.77 (s, 3H), 4.03 (s, 2H), 6.54 (dd, J_{min} = 1.8 Hz, J_{max} = 8.0 Hz, 1H), 7.20 (t, J = 8.0 Hz, 1H), 7.32-7.45 (m, 4H), 7.63 (t, J = 2.0 Hz, 1H), 8.31 (d, J = 7.2 Hz, 1H), 8.48 (s, 1H), 9.70 (s, 1H) ppm; ^{13}C NMR (100 MHz, DMSO-d$_6$): δ 25.92, 54.88, 104.23, 106.81, 111.06, 115.22, 126.19, 126.97, 127.97, 129.24, 131.22, 132.12, 136.60, 141.82, 156.48, 157.69, 159.31, 159.55 ppm; HRMS (ESI) m/z calculated for C$_{18}$H$_{16}$N$_3$OS ([M+H]$^+$) 322.10141, found: 322.10098. Anal. C$_{18}$H$_{15}$N$_3$OS (C, H, N).

*4.1.1.2. 2-(3-Chloroanilino)-5H-benzothiopyrane[4,3-d]pyrimidine (**2**).* Yield: 30%; m. p. 159-160 °C; ^{1}H NMR (400 MHz, DMSO-d$_6$): δ 4.04 (s, 2H), 6.99 (dd, J_{min} = 1.4 Hz, J_{max} = 8.0 Hz 1H), 7.33 (t, J = 8.2 Hz, 1H), 7.37-7.47 (m, 3H), 7.72 (dd, J_{min} = 1.4 Hz, J_{max} = 8.0 Hz, 1H), 8.06 (t, J = 2.2 Hz, 1H), 8.29 (d, J = 8.0 Hz, 1H), 8.53 (s, 1H), 9.95 (s, 1H) ppm; ^{13}C NMR (100 MHz, DMSO-d$_6$): δ 25.90, 115.81, 116.90, 117.77, 120.69, 126.23, 126.96, 127.99, 130.15, 131.32, 131.95, 132.96, 136.68, 142.16, 156.46, 157.84, 159.01 ppm; HRMS (ESI) m/z calculated for C$_{17}$H$_{13}$ClN$_3$S ([M+H]$^+$) 326.05187, found 326.05103. Anal. C$_{17}$H$_{12}$ClN$_3$S (C, H, N).

*4.1.1.3. 2-(3-Bromoanilino)-5H-benzothiopyrane[4,3-d]pyrimidine (**3**).* Yield: 30%; m. p. 178-179 °C; ^{1}H NMR (400 MHz, DMSO-d$_6$): δ 4.03 (s, 2H), 7.11 (dd, J_{min} = 2.0 Hz, J_{max} = 7.6 Hz, 1H), 7.26 (t, J = 8.0 Hz, 1H), 7.37-7.40 (m, 1H), 7.43-7.44 (m, 2H), 7.74 (dd, J_{min} = 1.2 Hz, J_{max} = 8.4 Hz, 1H), 8.21 (t, J = 2.0 Hz, 1H), 8.28 (d, J = 7.6 Hz, 1H), 8.51 (s, 1H), 9.91 (s, 1H) ppm; ^{13}C NMR (100 MHz, DMSO-d$_6$): δ 25.89, 115.78, 117.27, 120.66, 121.52, 123.57, 126.20, 126.95, 127.97, 130.45, 131.31, 131.94, 136.67, 142.29, 156.48, 157.80, 158.97 ppm; HRMS (ESI) m/z calculated for C$_{17}$H$_{13}$BrN$_3$S ([M+H]$^+$) 370.00136, 371.99931, found 370.00084, 371.99873. Anal. C$_{17}$H$_{12}$BrN$_3$S (C, H, N).

*4.1.1.4. 2-(3-Fluoroanilino)-5H-benzothiopyrane[4,3-d]pyrimidine (**4**).* Yield: 35%; m. p. 141-143°C; ^{1}H NMR (400 MHz, DMSO-d_6): δ 4.04 (s, 2H), 6.76 (dt, J_{min} = 2.2 Hz, J_{max} = 8.4 Hz, 1H), 7.30-7.46 (m, 4H), 7.56 (dd, J_{min} = 1.8 Hz, J_{max} = 8.0 Hz, 1H), 7.85 (td, J_{min} = 2.2 Hz, J_{max} = 12.4 Hz, 1H), 8.28 (d, J = 7.2 Hz, 1H), 8.52 (s, 1H), 9.96 (s, 1H) ppm; ^{13}C NMR (100 MHz, DMSO-d_6): δ 25.91, 104.96 (d, $^2J_{CF}$ = 27 Hz), 107.41 (d, $^2J_{CF}$ = 22 Hz), 114.33, 115.81, 126.29, 126.97, 128.01, 130.10, 131.32, 131.99, 136.67, 142.54, 156.46, 157.88, 159.07, 162.34 (d, $^1J_{CF}$ = 239 Hz) ppm; HRMS (ESI) m/z calculated for $C_{17}H_{13}FN_3S$ ([M+H]$^+$) 310.08142, found 310.08051. Anal. $C_{17}H_{12}FN_3S$ (C, H, N).

*4.1.1.5. 2-(3-Trifluoromethylanilino)-5H-benzothiopyrane[4,3-d]pyrimidine (**5**).* Yield: 50%; m. p. 154-157 °C; ^{1}H NMR (400 MHz, DMSO-d_6): δ 4.05 (s, 2H), 7.29 (d, J = 7.6 Hz, 1H), 7.37-7.39 (m, 1H), 7.44-7.46 (m, 2H), 7.54 (t, J = 7.8 Hz, 1H), 7.96 (d, J = 8.4 Hz, 1H), 8.29 (d, J = 7.6 Hz, 1H), 8.48 (s, 1H), 8.54 (s, 1H), 10.09 (s, 1H) ppm; ^{13}C NMR (100 MHz, DMSO-d_6): δ 25.88, 114.38 (q, $^3J_{CF}$ = 4.0 Hz), 115.89, 117.28 (q, $^3J_{CF}$ = 4.0 Hz), 122.00, 124.40, (q, $^1J_{CF}$ = 271 Hz), 126.15, 126.90, 127.98, 129.33 (q, $^2J_{CF}$ = 31 Hz), 129.63, 131.37, 131.94, 136.72, 141.41, 156.65, 157.75, 159.00 ppm; HRMS (ESI) m/z calculated for $C_{18}H_{13}F_3N_3S$ ([M+H]$^+$) 360.07823, found 360.07759. Anal. $C_{18}H_{12}F_3N_3S$ (C, H, N).

*4.1.1.6. 8-Methoxy-2-(3-methoxyanilino)-5H-benzothiopyrane[4,3-d]pyrimidine (**6**).* Yield: 30%; m. p. 137-138 °C; ^{1}H NMR (400 MHz, DMSO-d_6): δ 3.76 (s, 3H), 3.84 (s, 3H), 4.02 (s, 2H), 6.53 (dd, J_{min} = 2.4 Hz, J_{max} = 7.8 Hz, 1H), 6.95-6.99 (m, 2H), 7.19 (t, J = 8.1 Hz, 1H), 7.33 (d, J = 8.6 Hz, 1H), 7.61 (s, 1H), 8.25 (d, J = 8.8 Hz, 1H), 8.41 (s, 1H), 9.62 (s, 1H) ppm; ^{13}C NMR (100 MHz, DMSO-d_6): δ 26.23, 54.98, 55.57, 111.32, 112.10, 113.86, 115.21, 116.71, 118.65, 121.78, 124.09, 127.87, 130.43, 131.13, 138.27, 153.31, 159.99, 160.87, 164.81 ppm; HRMS (ESI) m/z calculated for $C_{19}H_{18}N_3O_2S$ ([M+H]$^+$) 352.11197, found 352.11124. Anal. $C_{19}H_{17}N_3O_2S$ (C, H, N).

4.1.1.7. 8-Methoxy-2-(3-chloroanilino)-5H-benzothiopyrane[4,3-d]pyrimidine (7). Yield: 30%; m. p. 139-140 °C; ^{1}H NMR (400 MHz, DMSO-d$_6$): δ 3.83 (s, 3H), 4.03 (s, 2H), 6.96-7.00 (m, 3H), 7.32 (t, *J* = 8.0 Hz, 1H), 7.72 (dd, J_{min} = 1.2 Hz, J_{max} = 8.4 Hz, 1H), 8.05 (t, *J* = 2.0 Hz, 1H), 8.22 (d, *J* = 8.8 Hz, 1H), 8.45 (s, 1H), 9.87 (s, 1H) ppm; ^{13}C NMR (100 MHz, DMSO-d$_6$): δ 26.15, 55.62, 112.29, 112.98, 114.65, 116.83, 117.69, 120.58, 124.66, 128.66, 130.15, 132.96, 138.61, 142.28, 155.97, 157.88, 158.95, 161.42 ppm; HRMS (ESI) m/z calculated for C$_{18}$H$_{15}$ClN$_3$OS ([M+H]$^+$) 356.06244, found 356.06189. Anal. C$_{18}$H$_{14}$ClN$_3$OS (C, H, N).

4.1.1.8. 8-Methoxy-2-(3-bromoanilino)-5H-benzothiopyrane[4,3-d]pyrimidine (8). Yield: 30%; m. p. 126-127 °C; ^{1}H NMR (400 MHz, DMSO-d$_6$): δ 3.83 (s, 3H), 4.02 (s, 2H), 6.93-6.99 (m, 2H), 7.11 (d, *J* = 7.6 Hz, 1H), 7.26 (t, *J* = 8.0 Hz, 1H), 7.69-7.78 (m, 2H), 8.20-8.25 (m, 1H), 8.44 (s, 1H), 9.84 (s, 1H) ppm; ^{13}C NMR (100 MHz, DMSO-d$_6$): δ 26.11, 55.59, 112.08, 112.75, 114.24, 119.87, 120.85, 124.48, 124.79, 128.34, 128.86, 138.41, 139.57, 141.89, 155.91, 157.88, 159.06, 161.35 ppm; HRMS (ESI) m/z calculated for C$_{18}$H$_{15}$BrN$_3$OS ([M+H]$^+$) 400.01192, 402.00987, found 400.01126, 402.00894. Anal. C$_{18}$H$_{14}$BrN$_3$OS (C, H, N).

4.1.1.9. 8-Methoxy-2-(3-fluoroanilino)-5H-benzothiopyrane[4,3-d]pyrimidine (9). Yield: 30%; m. p. 152-153 °C, ^{1}H NMR (400 MHz, DMSO-d$_6$): δ 3.82 (s, 3H), 4.03 (s, 2H), 6.75 (t, *J* = 7.6 Hz, 1H), 6.98-7.00 (m, 2H), 7.31-7.34 (m, 1H), 7.54 (d, *J* = 7.2 Hz, 1H), 7.82-7.85 (m, 1H); 8.23 (d, *J* = 7.6 Hz, 1H), 8.44 (s, 1H), 9.87 (s, 1H) ppm; ^{13}C NMR (100 MHz, DMSO-d$_6$): δ 26.22, 55.57, 104.61 (d, $^2J_{CF}$ = 25 Hz), 106.82 (d, $^2J_{CF}$ = 21 Hz), 112.14, 114.28, 119.88, 124.47, 124.72, 126.14, 128.23, 128.81, 138.43, 139.62, 155.876, 157.79, 159.04, 161.03 (d, $^1J_{CF}$ = 242 Hz) ppm; HRMS (ESI) m/z calculated for C$_{18}$H$_{15}$FN$_3$OS ([M+H]$^+$) 340.09199, found 340.09127. Anal. C$_{18}$H$_{14}$FN$_3$OS (C, H, N).

4.1.1.10. 8-Methoxy-2-(3-trifluoromethylanilino)-5H-benzothiopyrane[4,3-d]pyrimidine (10). Yield: 35%; m. p. 149-150 °C; ^{1}H NMR (400 MHz, DMSO-d$_6$): δ 3.84 (s, 3H), 4.04 (s, 2H), 6.94 (d, *J* = 8.4 Hz, 1H), 7.00 (s, 1H), 7.28 (d, *J* = 7.2 Hz, 1H), 7.53 (t, *J* = 7.6 Hz, 1H), 7.97 (d, *J* =

7.6 Hz, 1H), 8.23 (d, J = 8.4 Hz, 1H), 8.44 (s, 1H), 8.47 (s, 1H), 10.01 (s, 1H) ppm; ^{13}C NMR (100 MHz, DMSO-d$_6$): δ 26.12, 56.26, 112.28, 112.88, 114.31 (q, $^3J_{CF}$ = 4.0 Hz), 114.75, 117.16 (q, $^3J_{CF}$ = 4.0 Hz), 121.93, 124.41 (q, $^1J_{CF}$ = 271 Hz), 124.63, 128.57, 129.31 (q, $^2J_{CF}$ = 31 Hz), 129.62, 138.66, 141.51, 156.13, 157.79, 158.94, 161.45 ppm; HRMS (ESI) m/z calculated for C$_{19}$H$_{15}$F$_3$N$_3$OS ([M+H]$^+$) 390.08879, found 390.08798. Anal. C$_{19}$H$_{14}$F$_3$N$_3$OS (C, H, N).

*4.1.1.11. 8-Chloro-2-(3-methoxyanilino)-5H-benzothiopyrane[4,3-d]pyrimidine (**11**).* Yield: 35%; m. p. 166-167 °C; ^{1}H NMR (400 MHz, DMSO-d$_6$): δ 3.77 (s, 3H), 4.07 (s, 2H), 6.54 (dd, J_{min} = 2.2 Hz, J_{max} = 7.8 Hz, 1H), 7.20 (t, J = 8.2 Hz, 1H), 7.32 (dd, J_{min} = 1.2 Hz, J_{max} = 8.0 Hz, 1H), 7.46 (dd, J_{min} = 2.2 Hz, J_{max} = 8.6 Hz, 1H), 7.57-7.59 (m, 2H), 8.27 (d, J = 8.4 Hz 1H), 8.49 (s, 1H), 9.77 (s, 1H) ppm; ^{13}C NMR (100 MHz, DMSO-d$_6$): δ 25.90, 54.89, 104.27, 106.95, 111.11, 114.83, 126.28, 127.21, 128.45, 129.25, 130.92, 135.76, 138.92, 141.69, 156.68, 156.87, 159.30, 159.53 ppm; HRMS (ESI) m/z calculated for C$_{18}$H$_{15}$ClN$_3$OS ([M+H]$^+$) 356.06244, found 356.06201. Anal. C$_{18}$H$_{14}$ClN$_3$OS (C, H, N).

*4.1.1.12. 8-Chloro-2-(3-chloroanilino)-5H-benzothiopyrane[4,3-d]pyrimidine (**12**)* Yield: 35%; m. p. 220-1221 °C; ^{1}H NMR (400 MHz, DMSO-d$_6$): δ 4.06 (s, 2H), 6.99 (dd, J_{min} = 1.8 Hz, J_{max} = 7.8 Hz, 1H), 7.32 (t, J = 8.0 Hz, 1H), 7.45 (dd, J_{min} = 2.4 Hz, J_{max} = 8.4 Hz, 1H), 7.57 (d, J = 2.0 Hz, 1H), 7.71 (dd, J_{min} = 2.4 Hz, J_{max} = 8.4 Hz, 1H), 7.99 (t, J = 2.0 Hz, 1H), 8.24 (d, J = 8.4 Hz, 1H), 8.52 (s, 1H), 9.95 (s, 1H) ppm; ^{13}C NMR (100 MHz, DMSO-d$_6$): δ 25.88, 115.44, 116.95, 117.83, 120.80, 126.32, 127.24, 128.46, 130.16, 130.75, 132.95, 135.88, 139.00, 142.03, 156.66, 157.04, 159.01 ppm; HRMS (ESI) m/z calculated for C$_{17}$H$_{12}$Cl$_2$N$_3$S ([M+H]$^+$) 360.01290, found 360.01217. Anal. C$_{17}$H$_{11}$Cl$_2$N$_3$S (C, H, N).

*4.1.1.13. 8-Chloro-2-(3-bromoanilino)-5H-benzothiopyrane[4,3-d]pyrimidine (**13**).* Yield: 45%; m. p. 212-213 °C; ^{1}H NMR (400 MHz, DMSO-d$_6$): δ 4.07 (s, 2H), 7.12 (dd, J_{min} = 1.8 Hz, J_{max} = 7.4 Hz, 1H), 7.26 (t, J = 8.0 Hz, 1H), 7.44 (dd, J_{min} = 2.4 Hz, J_{max} = 8.4 Hz, 1H), 7.57 (d, J = 2.0 Hz, 1H), 7.75 (dd, J_{min} = 1.2 Hz, J_{max} = 8.4 Hz, 1H), 8.15 (t, J = 1.8 Hz, 1H), 8.24 (d, J = 8.4 Hz, 1H), 8.52 (s,

1H), 9.93 (s, 1H) ppm; ^{13}C NMR (100 MHz, DMSO-d$_6$): δ 25.87, 115.14, 116,62, 117.32, 120.73, 123.68, 124.81, 126.28, 127.13, 128.36, 130.45, 132.64, 135.73, 138.86, 139.01, 142.17, 158.97 ppm; HRMS (ESI) m/z calculated for C$_{17}$H$_{12}$BrClN$_3$S ([M+H]$^+$) 403.96238, 405,96034, found 403.96274, 405.95975. Anal. C$_{17}$H$_{11}$BrClN$_3$S (C, H, N).

4.1.1.14. 8-Chloro-2-(3-fluoroanilino)-5H-benzothiopyrane[4,3-d]pyrimidine (14). Yield: 30%; m. p. 190-193 °C; ^{1}H NMR (400 MHz, DMSO-d$_6$): δ 4.08 (s, 2H), 6.77 (dt, J_{min} = 2.0 Hz, J_{max} = 8.4 Hz, 1H), 7.30-7.36 (m, 1H), 7.48 (dd, J_{min} = 2.0 Hz, J_{max} = 8.4 Hz, 1H), 7.53-7.56 (m, 1H), 7.59 (d, J = 2.0 Hz, 1H), 7.80 (td, J_{min} = 2.4 Hz, J_{max} = 9.4 Hz, 1H), 8.26 (d, J = 8.4 Hz, 1H), 8.53 (s, 1H), 10.00 (s, 1H) ppm; ^{13}C NMR (100 MHz, DMSO-d$_6$): δ   25.89, 105.18 (d, $^2J_{CF}$ = 26 Hz), 106.81 (d, $^2J_{CF}$ = 24 Hz), 114.37, 115.43, 126,39, 127.26, 128.47, 130.79, 134.60, 135.87, 139.00, 142,51, 156.66, 157.07, 159.13, 162.14 (d, $^1J_{CF}$ = 239 Hz) ppm; HRMS (ESI) m/z calculated for C$_{17}$H$_{12}$ClFN$_3$S ([M+H]$^+$) 344.04245, found 344.04197. Anal. C$_{17}$H$_{11}$ClFN$_3$S (C, H, N).

4.1.1.15. 8-Chloro-2-(3-trifluoromethylanilino)-5H-benzothiopyrane[4,3-d]pyrimidine (15). Yield: 35%; m. p. 165-170 °C; ^{1}H NMR (400 MHz, DMSO-d$_6$): δ 4.08 (s, 2H), 7.29 (d, J = 7.6 Hz, 1H), 7.42 (dd, J_{min} = 2.1 Hz, J_{max} = 8.6 Hz, 1H), 7.53 (t, J = 7.6 Hz, 1H), 7.57 (d, J = 2.0 Hz, 1H), 7.98 (d, J = 8.0 Hz, 1H), 8.24 (d, J = 8.4 Hz, 1H), 8.38 (s, 1H), 8.54 (s, 1H), 10.11 (s, 1H) ppm; ^{13}C NMR (100 MHz, DMSO-d$_6$): δ 25.85, 114.44 (q, $^3J_{CF}$ = 4.0 Hz), 115.52, 117.36 (q, $^3J_{CF}$ = 4.0 Hz), 122.04, 124.35 (q, $^1J_{CF}$ = 271 Hz), 126.20, 127.23, 128.36, 129.32 (q, $^2J_{CF}$ = 30 Hz), 129.64, 130.72, 135.91, 139.04, 141.28, 156.81, 156.95, 158.99 ppm; HRMS (ESI) m/z calculated for C$_{18}$H$_{12}$ClF$_3$N$_3$S ([M+H]$^+$) 394.03926, found 394.03883. Anal. C$_{18}$H$_{11}$ClF$_3$N$_3$S (C, H, N).

4.1.1.16. 2-(3,4-Dimethoxyanilino)-5H-benzothiopyrane[4,3-d]pyrimidine (16). Yield: 40%; m. p. 148-149 °C; ^{1}H NMR (400 MHz, DMSO-d$_6$): δ 3.72 (s, 3H), 3.78 (s, 3H), 4.01 (s, 2H), 6.91 (d, J = 8.8 Hz, 1H), 7.26 (dd, J_{min} = 2.2 Hz, J_{max} = 8.6 Hz, 1H), 7.36-7.43 (m, 3H), 7.63 (d, J = 1.2 Hz, 1H), 8.31 (d, J = 7.6 Hz, 1H), 8.44 (s, 1H), 9.51 (s, 1H) ppm; ^{13}C NMR (100 MHz, DMSOd$_6$): δ 25.94, 55.29, 55.87, 104.27, 110.54, 112.37, 114.59, 126.12, 126.95, 127.93, 131.14, 132.22, 134.34,

136.56, 143.61, 148.53, 156.54, 157.55, 159.42 ppm; HRMS (ESI) m/z calculated for $C_{19}H_{18}N_3O_2S$ ([M+H]$^+$) 352.11197, found 352.11067. Anal. $C_{19}H_{17}N_3O_2S$ (C, H, N).

*4.1.1.17. 2-(3,4,5-Trimethoxyanilino)-5H-benzothiopyrane[4,3-d]pyrimidine (**17**).* Yield: 30%; m. p. 176-178 °C; ^{1}H NMR (400 MHz, DMSOd$_6$): δ 3.63 (s, 3H), 3.79 (s, 6H), 4.03 (s, 2H), 7.30 (s, 2H), 7.35-7.38 (m, 1H), 7.43-7.44 (m, 2H), 8.34 (d, *J* = 7.2 Hz, 1H), 8.47 (s, 1H), 9.58 (s, 1H) ppm; ^{13}C NMR (100 MHz, DMSO-d$_6$): δ 25.92, 55.61 (2C), 60.13, 96.30, 114.99 (2C), 126.07, 126.91, 127.96, 131.24, 131.99, 132.19, 136.63, 136.78, 152.65 (2C), 156.64, 157.50, 159.26 ppm; HRMS (ESI) m/z calculated for $C_{20}H_{20}N_3O_3S$ ([M+H]$^+$) 382.12254, found 382.12198. Anal. $C_{20}H_{19}N_3O_3S$ (C, H, N).

*4.1.1.18. 8-Methoxy-2-(3,4-dimethoxyanilino)-5H-benzothiopyrane[4,3-d]pyrimidine (**18**).* Yield: 35%; m. p. 204-205 °C; ^{1}H NMR (400 MHz, DMSO-d$_6$): δ 3.69 (s, 3H), 3.76 (s, 3H), 3.78 (s, 3H), 3.97 (s, 2H), 6.77 (dd, J_{min} = 2.2 Hz, J_{max} = 8.6 Hz, 1H), 6.85 (dd, J_{min} = 2.4 Hz, J_{max} = 8.8 Hz, 1H), 6.91-6.93 (m, 2H), 7.02 (d, *J* = 2.4 Hz, 1H), 7.79 (d, J = 8.8 Hz, 1H), 8.23 (s, 1H), 9.52 (s, 1H) ppm; ^{13}C NMR (100 MHz, DMSO-d$_6$): δ 25.92, 55.52, 55.57, 60.01, 111.73, 112.00, 114.87, 119.56, 126.04, 127.84, 132.12, 133.00, 137.99, 138.03, 146.54, 148.68, 151.64, 156.61, 157.48, 159.08 ppm; HRMS (ESI) m/z calculated for $C_{20}H_{20}N_3O_3S$ ([M+H]$^+$) 382.12254, found 382.12178. Anal. $C_{20}H_{19}N_3O_3S$ (C, H, N).

*4.1.1.19. 8-Methoxy-2-(3,4,5-trimethoxyanilino)-5H-benzothiopyrane[4,3-d]pyrimidine (**19**).* Yield: 30%; m. p. 166-168 °C; ^{1}H NMR (400 MHz, DMSO-d$_6$): δ 3.62 (s, 3H), 3.74 (s, 6H), 3.79 (s, 3H), 4.01 (s, 2H), 6.94 (dd, J_{min} = 2.4 Hz, J_{max} = 8.8 Hz, 1H), 6.99 (d, *J* = 2.4 Hz, 1H), 7.28 (s, 2H), 8.27 (d, *J* = 8.4 Hz, 1H), 8.40 (s, 1H), 9.49 (s, 1H) ppm; ^{13}C NMR (100 MHz, DMSO-d$_6$): δ 25.93, 55.28, 55.54 (2C), 60.03, 96.28, 114.92 (2C), 126.00, 126.82, 127.93, 131.14, 132.02, 132.14, 136.56, 136.71, 151.97 (2C), 156.58, 157.45, 159.22 ppm; HRMS (ESI) m/z calculated for $C_{21}H_{22}N_3O_4S$ ([M+H]$^+$)412.13310, found 412.13274. Anal. $C_{21}H_{21}N_3O_4S$ (C, H, N).

*4.1.1.20. 8-Chloro-2-(3,4-dimethoxyanilino)-5H-benzothiopyrane[4,3-d]pyrimidine (**20**).* Yield: 35%; m. p. 180-183 °C; ^{1}H NMR (400 MHz, DMSO-d$_6$): δ 3.75 (s, 3H), 3.78 (s, 3H), 4.04 (s, 2H),

6.90 (d, J = 8.8 Hz, 1H), 7.23 (dd, J_{min} = 2.2 Hz, J_{max} = 9.0 Hz, 1H), 7.44 (dd, J_{min} = 1.8 Hz, J_{max} = 8.6 Hz, 1H), 7.55-7.60 (m, 2H), 8.27 (d, J = 8.4 Hz, 1H), 8.44 (s, 1H), 9.53 (s, 1H) ppm; ^{13}C NMR (100 MHz, DMSO-d$_6$): δ 25.92, 55.32, 55.85, 104.33, 110.64, 112.35, 114.18, 122.31, 126.20, 127.16, 128.42, 131.02, 134.18, 135.65, 138.86, 143.69, 148.54, 156.71, 159.41 ppm; HRMS (ESI) m/z calculated for $C_{19}H_{17}ClN_3O_2S$ ([M+H]$^+$) 386.07300, found 386.07244. Anal. $C_{19}H_{16}ClN_3O_2S$ (C, H, N).

*4.1.1.21. 8-Chloro-2-(3,4,5-trimethoxyanilino)-5H-benzothiopyrane[4,3-d]pyrimidine (**21**).* Yield: 30%; m. p. 162-165 °C; ^{1}H NMR (400 MHz, DMSOd$_6$): δ 3.63 (s, 3H), 3.79 (s, 6H), 4.06 (s, 2H), 7.26 (s, 2H), 7.45 (dd, J_{min} = 1.8 Hz, J_{max} = 8.2 Hz, 1H), 7.58 (d, J = 2.0 Hz, 1H), 8.3 (d, J = 8.4 Hz, 1H), 8.48 (s, 1H), 9.62 (s, 1H) ppm; ^{13}C NMR (100 MHz, DMSOd$_6$): δ 25.93, 55.26, 55.63 (2C), 96.31, 114.95 (2C), 126.03, 126.86, 127.91, 131.18, 132.01, 132.15, 136.58, 136.72, 152.63 (2C), 156.65, 157.47, 159.24 ppm; HRMS (ESI) m/z calculated for $C_{20}H_{19}ClN_3O_3S$ ([M+H]$^+$) 416.08356, found 416.08287. Anal. $C_{20}H_{18}ClN_3O_3S$ (C, H, N).

4.2. Biological evaluation

4.2.1.   Inhibition growth assay.

HeLa (human cervix adenocarcinoma cells) and A-431 (skin carcinoma squamous cells) were grown in Nutrient Mixture F-12 [HAM] (Sigma Chemical Co.) and Dulbecco's modified Eagle's medium (Sigma Chemical Co.) respectively. MSTO-211H (human biphasic mesothelioma cells) were grown in RPMI 1640 (Sigma Chemical Co.) supplemented with 2.4 g/L Hepes, 0.11 g/L Na-pyruvate. 10% Heat-inactivated fetal calf serum (Invitrogen), 100 U/mL penicillin, 100 mg/mL streptomycin and 0.25 mg/mL amphotericin B (Sigma Chemical Co.) were added to the media. HUVECs (human umbilical vein endothelial cells) were purchased from Lonza Ltd. and maintained as recommended. The cells were cultured at 37 °C in a moist atmosphere of 5% carbon dioxide in air.

Cells (3×10^4) were seeded into each well of a 24-well cell culture plate. After incubation for 24 h, various concentrations of the test agents were added to the complete medium and cells were incubated for a further 72 h. A trypan blue assay was performed to determine cell viability. Cytotoxicity data were expressed as GI_{50} values, i.e., the concentration of the test agent inducing 50% reduction in cell number compared with control cultures.

4.2.2.   KDR activity assay.

The KDR kinase activity was assessed by using the Z′-LYTE-Tyr1 Peptide assay kit (Invitrogen), according to the procedures recommended by the manufacturer. Briefly, assays were performed in a total of 60 µL in 96-well plates (Optiplate-96, black, Perkin Elmer) using fluorescence resonance energy transfer technology. A Tyr1 substrate (coumarin-fluorescein double labeled peptide) at 2.0 μM was incubated for 1 h at room temperature with 0.7 µg/mL KDR (Life Technologies), 10 µM ATP, and test agents at room temperature in kinase buffer. Then, 15.0 μL of the development reagent were added to each well and samples were incubated for further 1 hour. At the end, 15 μL of the stop reagent were added and fluorescence signal was detected by using a Victor 1460 Multilabel Counter (Perkin Elmer). The fluorescence emission was read at 445 nm and 520 nm (excitation wavelength = 400 nm) and the percentage of phosphorylation was determined as indicated by the manufacture.

4.2.3.   In vitro kinases enzymatic inhibition.

The screening of compound **16** on a set of 6 human kinases (AurA/Aur2 kinase, CDC2/CDK1, EGFR kinase, PDGFRb kinase, RAF-1 kinase, Src kinase) was performed by CEREP (France), according to the company's standard operating procedures (Figure 1, Tables S1a-S1b).

4.3.   Molecular Modeling

The latest version of the docking software AutoDock Vina (version 1.1.2) [28] in conjunction with the graphical user interface AutoDockTools (ADT) [35] was used to perform the ensemble docking calculations. AutoDock Vina docking performances and accuracy are assured by a Lamarckian algorithm and an empirical binding free energy force field. The VEGFR-2 X-ray structures used for

the experiment had the following PDB codes: 1YWN, 2P2H, 2XIR, 3BE2, 3EWH, 3VHE, 3VNT, 3VO3, 3WZD, 3WZE, 4AG8, and 4ASE. The 3D structures were prepared using the Protein Preparation Wizard of the Maestro suite (Schrödinger Release 2017-2) [36], which assigns bond orders, adds hydrogen atoms, deletes water molecules and generates the appropriate protonation states. Maestro was also employed to superimpose all the enzyme structures to the 1YWN structure. The 2D Sketcher tool of Maestro was used to build compound **16**. The ligand protonation and tautomeric states, as well as its geometry, were optimized through LigPrep, part of the Maestro suite. Afterwards, both the ligand and the receptors had to be converted to the pdbqt format. The latter is very similar to a standard pdb but it includes ′Q′ (partial charges) and ′T′ atom types. Each atom has one line, and special keywords are used if some are required to be flexible in the docking calculations. Preparing the structures involves ensuring that its atoms are assigned the correct atom types, adding Gasteiger charges if necessary, merging non-polar hydrogens, detecting aromatic carbons, and setting up the ′torsion tree′ in the case of ligands. Therefore, the python scripts prepare_receptor4.py and prepare_ligand4.py, part of ADT, were employed applying the standard settings. After the preparation, the docking was performed using the default settings of Vina, setting the midpoint of the putative binding site as the center of the box. The length of the box was fixed at 23 Å for the X, Y and Z coordinates.

The electrostatic potentials of compounds **5** and **16** were calculated by means of the Jaguar suite within the Schrödinger package (Schrödinger Release 2017-2) [37] and mapped onto their electron density. The isovalue of 0.0002 electron/Bhor3 was chosen for the definition of the density surface, while the electrostatic potential was computed using the 6-31G* basis set with a scale of -20.0 (red) to 35.0 kcal/mol (blue).

AUTHOR INFORMATION

Corresponding Authors

Prof. Sabrina Taliani *e-mail: sabrina.taliani@unipi.it, Prof. Sandro Cosconati *e-mail: sandro.cosconati@unicampania.it

Author Contributions

The manuscript was written through contributions of all authors. All authors have given approval to the final version of the manuscript.

Appendix A. Supplementary data.

Supplementary data related to this article for publication on line.

References

[1]   T.A. Baudino, Targeted Cancer Therapy: The Next Generation of Cancer Treatment, Curr. Drug. Discov. Technol. 12 (2015) 3-20.

[2]   C. Brown, Targeted therapy: An elusive cancer target, Nature 537 (2016) S106-8.

[3]   R.K. Jain, Normalization of tumor vasculature: an emerging concept in antiangiogenic therapy. Science 307 (2005) 58-62.

[4]   N. Maishi, K. Hida, Tumor endothelial cells accelerate tumor metastasis, Cancer Sci. 108 (2017) 1921-1926.

[5]   D. Ribatti, Judah Folkman, a pioneer in the study of angiogenesis, Angiogenesis 11 (2008) 3-10.

[6]   K. Sivaraman Siveen, P., Kirti, R. Krishnankutty, S. Kuttikrishnan, M. Tsakou, F.Q. Alali, S. Dermime, R.M. Mohammad, S. Uddin, Vascular Endothelial Growth Factor (VEGF) Signaling in Tumour Vascularization: Potential and Challenges, Curr. Vasc. Pharmacol. 15 (2017) 12-24.

[7] R. Roskoski, VEGF receptor protein-tyrosine kinases: structure and regulation, Biochem. Biophys. Res. Commun. 375 (2008) 287-291.

[8] M. Shibuya, Vascular Endothelial Growth Factor (VEGF) and Its Receptor (VEGFR) Signaling in Angiogenesis: A Crucial Target for Anti- and Pro-Angiogenic Therapies, Genes Cancer 2 (2011) 1097-1105.

[9] E. Cabebe, G.A. Fisher, Clinical trials of VEGF receptor tyrosine kinase inhibitors in pancreatic cancer, Expert Opin. Invest. Drugs 16 (2007) 467-476.

[10] F.W. Peng, D.K. Liu, Q.W. Zhang, Y.G. Xu, L. Shi, VEGFR-2 inhibitors and the therapeutic applications thereof: a patent review (2012-2016), Expert Opin. Ther. Pat. 27 (2017) 987-1004.

[11] R.L. Bitting, P. Healy, P.A. Creel, J. Turnbull, K. Morris, S.Y. Wood, H.I. Hurwitz, M.D. Starr, A.B. Nixon, A.J. Armstrong, D.J. George, A phase Ib study of combined VEGFR and mTOR inhibition with vatalanib and everolimus in patients with advanced renal cell carcinoma, Clin. Genitourin. Cancer 12 (2014) 241-250.

[12] S.A. Laurie, B.J. Solomon, L. Seymour, P.M. Ellis, G.D. Goss, F.A. Shepherd, M.J. Boyer, A.M. Arnold, P. Clingan, F. Laberge, D. Fenton, V. Hirsh, M. Zukin, M.R. Stockler, C.W. Lee, E.X. Chen, A. Montenegro, K. Ding, P.A. Bradbury, Randomised, double-blind trial of carboplatin and paclitaxel with daily oral cediranib or placebo in patients with advanced non-small cell lung cancer: NCIC Clinical Trials Group study BR29, Eur. J. Cancer 50 (2014) 706-712.

[13] P. Wu, T.E. Nielsen, M.H. Clausen, FDA-approved small-molecule kinase inhibitors, Trends Pharmacol. Sci. 36 (2015) 422–439.

[14] L.A. McDermott, M. Simcox, B. Higgins, T. Nevins, K. Kolinsky, M. Smith, H. Yang, J.K. Li, Y. Chen, J. Ke, N. Mallalieu, T. Egan, S. Kolis, A. Railkar, L. Gerber, K.C. Luk, RO4383596, an orally active KDR, FGFR, and PDGFR inhibitor: synthesis and biological evaluation, Bioorg. Med. Chem. 13 (2005) 4835-4841.

[15] X. N. Guo, L. Zhong, J. Z. Tan, J. Li, X.M. Luo, H.L. Jiang, F.J. Nan, L.P. Lin, X.W. Zhang, J. Ding, In vitro pharmacological characterization of TKI-28, a broad-spectrum tyrosine kinase inhibitor with anti-tumor and anti-angiogenic effects, Cancer Biol. Ther. 4 (2005) 1125-1132.

[16] J.C. Soria, J. Baselga, N. Hanna, S.A. Laurie, R. Bahleda, E. Felip, E. Calvo, J.P. Armand, F.A. Shepherd, C.T. Harbison, D. Berman, J.S. Park, S. Zhang, B. Vakkalagadda, J.F. Kurland, A.K. Pathak, R.S. Herbst, Phase I-IIa study of BMS-690514, an EGFR, HER-2 and -4 and VEGFR-1 to -3 oral tyrosine kinase inhibitor, in patients with advanced or metastatic solid tumours, Eur. J. Cancer 49 (2013) 1815-1824.

[17] P.A. Ple, F. Jung, S. Ashton, L. Hennequin, R. Laine, R. Morgentin, G. Pasquet, S. Taylor, Discovery of AZD2932, a new Quinazoline Ether Inhibitor with high affinity for VEGFR-2 and PDGFR tyrosine kinases, Bioorg. Med. Chem. Lett. 22 (2012) 262-266.

[18] S. Schenone, F. Bondavalli, M. Botta, Antiangiogenic agents: an update on small molecule VEGFR inhibitors, Curr. Med. Chem. 14 (2007) 2495-2516.

[19] F. Musumeci, M. Radi, C. Brullo, S. Schenone, Vascular endothelial growth factor (VEGF) receptors: drugs and new inhibitors, J. Med. Chem. 55 (2012) 10797-10822.

[20] S. Salerno, A. M. Marini, G. Fornaciari, F. Simorini, C. La Motta, S. Taliani, S. Sartini, F. Da Settimo, A.N. Garcia-Argaez, O. Gia, S. Cosconati, E. Novellino, P. D'Ocon, A. Fioravanti, P. Orlandi, G. Bocci, L. Dalla Via, Investigation of new 2-aryl substituted benzothiopyrano[4,3-d]pyrimidines as kinase inhibitors targeting vascular endothelial growth factor receptor 2, Eur. J. Med. Chem. 103 (2015) 29-43.

[21] J.M. Jimenez, J. G., H. Gao, Y.C. Moon, G. Brenchley, R. Knegtel, F. Pierard, Preparation of aminopyrimidine derivatives as inhibitors of protein kinases U.S. Patent No. 20,050,148,603, 2005.

[22] P.S. Sharma, R. Sharma, T. Tyagi, VEGF/VEGFR pathway inhibitors as anti-angiogenic agents: present and future, Curr. Cancer Drug Targets 11 (2011) 624-653.

[23] S. Kraege, K. Stefan, K. Juvale, T. Ross, T. Willmes, M. Wiese, The combination of quinazoline and chalcone moieties leads to novel potent heterodimeric modulators of breast cancer resistance protein (BCRP/ABCG2), Eur. J. Med. Chem. 117 (2016) 212-229.

[24] H. Zhong, J.P. Bowen, Recent advances in small molecule inhibitors of VEGFR and EGFR signaling pathways, Curr. Top. Med. Chem. 11 (2011) 1571-1590.

[25] A.M. Marini, F. Da Settimo, S. Salerno, C. La Motta, F. Simorini, S. Taliani, D. Bertini, O. Gia, L. Dalla Via, Synthesis and in vitro antiproliferative activity of new substituted benzo[30,20:5,6]thiopyrano[4,3-d]pyrimidines, J. Heterocycl.Chem. 45 (2008) 745-749.

[26] A. Morabito, E. De Maio, M. Di Maio, N. Normanno, F. Perrone, Tyrosine kinase inhibitors of vascular endothelial growth factor receptors in clinical trials: current status and future directions, Oncologist 11 (2006) 753-764.

[27] M. Carmena, W.C. Earnshaw, The cellular geography of aurora kinases, Nat. Rev. Mol. Cell Biol. 4 (2003) 842-854.

[28] O. Trott, A.J. Olson, AutoDock Vina: improving the speed and accuracy of docking with a new scoring function, efficient optimization, and multithreading, J. Comput. Chem. 31 (2010) 455-461.

[29] S. Cosconati, S. Forli, A.L. Perryman, R. Harris, R.; D.S. Goodsell, S.J. Olson, Virtual Screening with AutoDock: Theory and Practice, Expert Opin. Drug Discovery 5 (2010) 597-607.

[30] S. Cosconati, L. Marinelli, F.S. Di Leva, V. La Pietra, A. De Simone, F. Mancini, V. Andrisano, E. Novellino, D.S. Goodsell, A.J. Olson, Protein flexibility in virtual screening: the BACE-1 case study, J. Chem. Inf. Model. 52 (2012) 2697-2704.

[31] S. Cosconati, J.A. Hong, E. Novellino, K.S. Carroll, D.S. Goodsell, A.J. Olson, Structure-based virtual screening and biological evaluation of Mycobacterium tuberculosis adenosine 5'-phosphosulfate reductase inhibitors,m J. Med. Chem. 51 (2008) 6627-6630.

[32] V.J. Cee, A.C. Cheng, K. Romero, S. Bellon, C. Mohr, D.A. Whittington, A. Bak, J. Bready, S. Caenepeel, A. Coxon, H.L. Deak, J. Fretland, Y. Gu, B.L. Hodous, X. Huang, J.L. Kim, J. Lin, A.M. Long, H. Nguyen, P.R. Olivieri, V.F. Patel, L. Wang, Y. Zhou, P. Hughes, S. Geuns-Meyer, Pyridyl-pyrimidine benzimidazole derivatives as potent, selective, and orally bioavailable inhibitors of Tie-2 kinase, Bioorg. Med. Chem. Lett. 19 (2009) 424-427.

[33] E.F. Pettersen, T.D. Goddard, C.C. Huang, G.S. Couch, D.M. Greenblatt, E.C. Meng, T.E. Ferrin, UCSF Chimera--a visualization system for exploratory research and analysis, J. Comput. Chem. 25 (2004) 1605-1612.

[34] S. Mecozzi, A.P. West, D.A. Dougherty, Cation-pi interactions in aromatics of biological and medicinal interest: electrostatic potential surfaces as a useful qualitative guide, Proc. Natl. Acad. Sci. U. S. A. 93 (1996) 10566-10571.

[35] G.M. Morris, R. Huey, W. Lindstrom, M.F. Sanner, R.K. Belew, D.S. Goodsell, A.J. Olson, AutoDock4 and AutoDockTools4: Automated docking with selective receptor flexibility, J. Comput. Chem. 30 (2009) 2785-2791.

[36] Schrödinger Release 2017-2: Maestro, S., LLC, New York, NY, 2017.

[37] Schrödinger Release 2017-3: MS Jaguar, S., LLC, New York, NY, 2017